Letter

Topological superconductivity by engineering noncollinear magnetism in magnet/superconductor heterostructures: A realistic prescription for the two-dimensional Kitaev model

Pritam Chatterjee,[1,2,*] Sayan Banik,[3,*] Sandip Bera,[3] Arnob Kumar Ghosh,[1,2]
Saurabh Pradhan,[4] Arijit Saha,[1,2,†] and Ashis K. Nandy[3,‡]

[1]*Institute of Physics, Sachivalaya Marg, Bhubaneswar-751005, India*
[2]*Homi Bhabha National Institute, Training School Complex, Anushakti Nagar, Mumbai 400094, India*
[3]*School of Physical Sciences, National Institute of Science Education and Research, An OCC of Homi Bhabha National Institute, Jatni 752050, India*
[4]*Lehrstuhl für Theoretische Physik II, Technische Universität Dortmund Otto-Hahn-Str. 4, 44221 Dortmund, Germany*

(Received 7 March 2023; revised 20 October 2023; accepted 22 February 2024; published 11 March 2024)

We report on a realistic and rather general scheme where noncollinear magnetic textures proximitized with the most common *s*-wave superconductor can appear as the alternative to *p*-wave superconductor—the prime proposal to realize two-dimensional (2D) Kitaev model for topological superconductors (TSCs) hosting Majorana flat edge mode (MFEM). A general minimal Hamiltonian suitable for magnet/superconductor heterostructures reveals robust MFEM within the gap of Shiba bands due to the emergence of an effective "$p_x + p_y$"-type *p*-wave pairing, spatially localized at the edges of a 2D magnetic domain of spin spiral. We finally verify this concept by considering Mn (Cr) monolayer grown on an *s*-wave superconducting substrate Nb(110) under strain [Nb(001)]. In both 2D cases, the antiferromagnetic spin-spiral solutions exhibit robust MFEM at certain domain edges that is beyond the scope of the trivial extension of one-dimensional (1D) spin-chain model in 2D. This approach, particularly when the MFEM appears in the TSC phase for such heterostructure materials, offers a perspective to extend the realm of the TSC in 2D.

DOI: 10.1103/PhysRevB.109.L121301

Introduction. A strong quest for topological superconductors (TSCs) hosting Majorana zero-modes (MZMs) [1–9] has been accumulating an immense interest based on magnetic adatoms fabricated on top of an *s*-wave superconductor (SC) substrate [10–32]. These magnetic atoms in the presence of superconductivity lead to the formation of Yu-Shiba-Rusinov (YSR)/Shiba bands [10,11,33] inside the superconducting gap. The mini gap created within such bands plays a pivotal role in exhibiting topological MZMs [10,11,34–39] through phase transitions, akin to the one-dimensional Kitaev model (1D-KM) [1,4]. Generally, the corresponding features like the Shiba states and/or the MZMs are experimentally detected [40–46] in a 1D spin chain mimicking a trail of magnetic impurities when grown on an *s*-wave SC. It is essential to highlight that a transition from a 1D finite ferromagnetic (FM) spin-chain model with Rashba SOC to its two-dimensional (2D) counterpart (FM finite domain) reveals fresh and unique phenomena: the TSC phase in 1D is manifested through the emergence of MZMs [47,48] while a generalized "$p_x + ip_y$"-type pairing governing 2D TSC phase brings higher Chern numbers and dispersive chiral Majorana edge modes [49,50]. Preserving all essential terms in those models, this dimensional extension in the problem introduces unique and distinct physics beyond the scope of its 1D counterpart. Therefore, moving to 2D-KM, the prime proposal turns out to be the *p*-wave SCs and thus, there has been a growing consensus on realizing *p*-wave SCs in materials despite its rarity so far. A distinct signature of such TSCs is nondispersive Majorana flat edge modes (MFEMs) localized at edges of a 2D domain, which can be probed experimentally using scanning-tunneling microscopy (STM) and angle-resolved photo emission spectroscopy (ARPES).

Recently, theoretical proposals for the 2D-KM with topological gapless phase hosting MFEMs has been put forward by employing ($p_x + p_y$) SCs [51,52]. A few alternative schemes using inhomogeneous magnetic fields, various magnetic orders, etc., were also explored to generate different *p*-wave pairing [53–55]. Although a formal connection involving both model and real materials, manifesting similar behavior has never been proposed in this context. Hence, we can address the following intriguing questions that have not been answered so far to the best of our knowledge: (a) Can we architect and identify magnetic heterostructures where the spin-spiral (SS) solution in the presence of *s*-wave SC exhibits features of 2D-KM? (b) Is it possible to derive an effective continuum model consisting of an induced effective spin-orbit coupling (SOC) and Zeeman field to describe such system? (c) Finally, and the most importantly, can we identify prototype systems where the SS ground state exhibits gapless TSC phase hosting MFEM within a lattice model? By stabilizing the SS state in 2D films comprising of 3*d* transition metal (TM) monolayer and *s*-wave SC substrate may offer

*These authors contributed equally to this work.
†arijit@iopb.res.in
‡aknandy@niser.ac.in

the most promising platform for stabilizing the TSC phase in experiments.

In this letter, we first deal with the SS textures in 2D, mimicking spatially varying magnetic impurities proximitized with an s-wave SC. An effective $(p_x + p_y)$-SC pairing is identified for the SS propagating along [110] direction in a square domain, manifesting gapless TSC phase. Note, the signature of the TSC phase, i.e., the nondispersive MFEMs cannot be obtained by straightforward generalization of a 1D system [11]. The interplay between the SS state and s-wave SC in our minimal model leads to the emergence of a distinctive "$p_x + p_y$"-type SC pairing, supporting the existence of a gapless topological superconducting phase in 2D. At the end, the designed TM/SC heterostructures must reveal SS ground state. We design potential material candidates: one monolayer of Mn and Cr on Nb(110) and Nb(001) SC substrates, respectively. Experimentally observed in-gap YSR band in Mn/Nb(110) [56] is well reproduced within our minimal model, owing to the proximity induced SC in the antiferromagnetic (AFM) state. By looking at other aspects of 2D noncollinear magnets [57–59], we apply uniform biaxial strain for engineering AFM-SS state as the ground state in Mn/Nb(110). The AFM-SS within a lattice model reveals TSC phase hosting MFEM. The TSC phase is further observed in another example, unstrained Cr/Nb(001). Hence, such real materials platform adds significant merit to the problem we are dealing with.

Formulation of 2D Kitaev continuum model. Within a continuum model, we first propose a general route to design 2D gapless TSC phase via engineering SS textures, when proximitized with an s-wave SC. The 2D model Hamiltonian for locally varying magnetic impurities reads in the Nambu spinor form $\Psi(\mathbf{r}) = (c_{\mathbf{r},\uparrow}, \quad c_{\mathbf{r},\downarrow}, \quad c^{\dagger}_{\mathbf{r},\downarrow}, \quad -c^{\dagger}_{\mathbf{r},\uparrow})^{\mathrm{T}}$ as $\mathcal{H}_{2\mathrm{D}} = \int d\mathbf{r}\Psi^{\dagger}(\mathbf{r})\, H\, \Psi(\mathbf{r})$, where $c_{\mathbf{r},\uparrow(\downarrow)}$ represents the quasiparticle annihilation operator for the up (down) spin at $\mathbf{r} = (x, y)$. The first quantized form of this Hamiltonian reads

$$H = -\tfrac{1}{2}\nabla^2\tau_z - J\mathbf{S}(\mathbf{r})\cdot\boldsymbol{\sigma} + \Delta_0\tau_x - \mu\tau_z. \tag{1}$$

For simplicity, we consider $\hbar = 1$ and $m = 1$. The Pauli matrices σ and τ acts on the spin and particle-hole subspace, respectively. J, Δ_0, and μ denote the local exchange-interaction strength between the magnetic impurity spin and electrons in the SC, the s-wave order parameter, and the chemical potential, respectively. We assume the impurity spins to be classical and confined in the xy plane with magnitude $|\mathbf{S}| = 1$. Therefore, spin vector $\mathbf{S}(\mathbf{r})$ can be locally described as $\mathbf{S}(\mathbf{r}) = |\mathbf{S}|(\cos[\phi(\mathbf{r})], \quad \sin[\phi(\mathbf{r})], \quad 0)$ with $\phi(\mathbf{r})$ the angle between two adjacent spins. By a unitary transformation $U = e^{-\frac{i}{2}\phi(\mathbf{r})\sigma_z}$, an effective low-energy Hamiltonian $\tilde{H} = U^{\dagger}HU$ in 2D becomes

$$\tilde{H} = -\frac{1}{2}\sum_{r_i=x,y}\left[\nabla^2_{r_i} - \left(\frac{\partial\phi}{\partial r_i}\right)^2 - \left(i\frac{\partial\phi}{\partial r_i}\nabla_{r_i} + i\nabla_{r_i}\frac{\partial\phi}{\partial r_i}\right)\sigma_z\right]\tau_z - J\sigma_x + \Delta_0\tau_x - \mu\tau_z. \tag{2}$$

Note, the similar mapping was reported for 1D spin-chain model in case of Majorana bound-state solution [60].

Henceforth, we assume that the SS is propagating along the diagonal of a square domain as depicted in Fig. 1, effectively

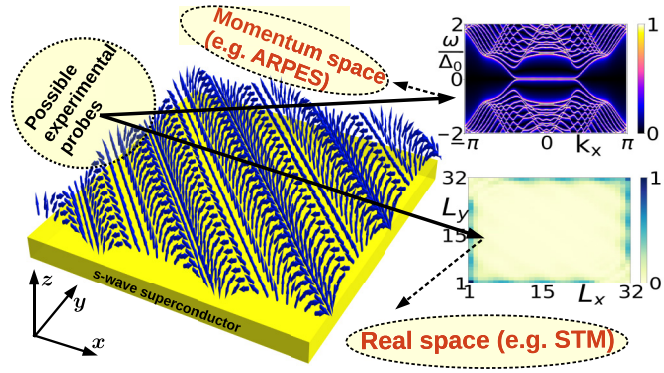

FIG. 1. The schematic setup of our model, a 2D square lattice with SS state placed on the surface of an s-wave SC. Two possible experimental schemes to probe MFEM: the momentum-space probe (e.g., ARPES), measures the spectral function as a signature of the MFEM and the real space probe (e.g., STM), measures the spatial distribution of the MFEM at edges, see the corresponding right images.

along [110] direction. The angle $\phi(\mathbf{r}) = \mathbf{g}\cdot\mathbf{r} = (g_x x + g_y y)$ defines the angle between two adjacent spins along the SS propagation direction where g_x and g_y values control the SS period and propagation direction. Generally, for $|g_x| \neq |g_y|$, one finds an asymmetric spin texture where the SS propagates neither [110] nor [1$\bar{1}$0] directions and the Hamiltonian $\tilde{H}$ in Eq. (2) can be rewritten in the momentum space as

$$\tilde{H}(\mathbf{k}) = \xi_{\mathbf{k},\mathbf{g}}\tau_z + \tfrac{1}{2}\mathbf{g}\cdot\mathbf{k}\,\sigma_z\tau_z + J\sigma_x + \Delta_0\tau_x, \tag{3}$$

where, $\xi_{\mathbf{k},\mathbf{g}} = \frac{1}{2}(\mathbf{k}^2 + \mathbf{g}^2) - \mu$. The second term represents an effective SOC, resulting from the spin texture in our model. Although the nature of such SOC is quite nontrivial as it originates from the spin texture, it can interestingly show a gapless TSC phase in the presence of Zeeman-like field of strength J along the x direction. We obtain the spectrum for the Hamiltonian $\tilde{H}(\mathbf{k})$ Eq. (3) as $E_{r,s}(\mathbf{k},\mathbf{g}) = r\sqrt{J^2 + \Delta_0^2 + \xi^2_{\mathbf{k},\mathbf{g}} + \frac{1}{4}\mathbf{k}\cdot\mathbf{g} + sF(\mathbf{k},\mathbf{g})}$, where $r, s = \pm$ and $F(\mathbf{k},\mathbf{g}) = \sqrt{[(\mathbf{k}\cdot\mathbf{g})^2 + 4J^2]^2\xi^2_{k,g} + 4J^2\Delta_0^2}$. Following the gap-closing condition corresponding to the two lowest energy bands, the critical value of J becomes $J_c(\mathbf{g}) = \sqrt{\Delta_0^2 + (\mu - \mathbf{g}^2/2)^2}$. The SS period now can be manifested like $T = \pi/|\mathbf{g}| = \pi/\sqrt{g_x^2 + g_y^2}$ [60]. Hence, in case of $|g_x| = |g_y| = g$, the period turns out to be $T = \pi/\sqrt{2}g$. Naively, the SS solution is governed by the RKKY-type (Ruderman-Kittel-Kasuya-Yosida) exchange frustration and if the period of SS is set by the Fermi momentum $\mathbf{k}_F$, then $T = \pi/|\mathbf{g}| = \pi/|\mathbf{k}_F|$ [12–14,60]. In such case, the topological transition occurs at $J_c = \Delta_0$ so that $\mu = |\mathbf{k}_F|^2/2$. However, in real TM/SC systems, the SS solution is the outcome of a complex interplay of material-dependent parameters: the exchange coupling constants $\mathcal{J}_{ij}$'s; the Dzyaloshinskii-Moriya Interactions (DMIs) $\mathbf{D}_{ij}$'s; and the uniaxial magneto crystalline anisotropy $\mathcal{K}$.

The band structure of this system has been analyzed using the lattice version of the Hamiltonian $\tilde{H}(\mathbf{k})$ defined as $\tilde{H}_{\mathrm{L}}(\mathbf{k})$, see Eq. (S1) in the Supplemental Material (SM), Sec. S1

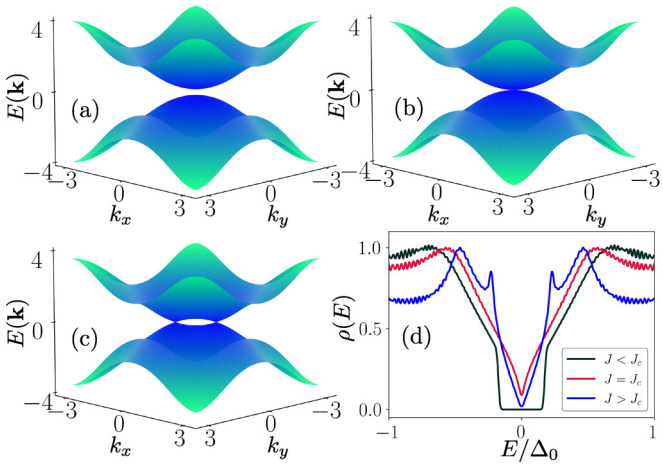

FIG. 2. The bulk band structures of the Hamiltonian $\tilde{H}_{\rm L}(\mathbf{k})$ in the k_x-k_y plane is depicted for (a) the trivially gapped SC phase $J < J_c$ $(= 1.6\Delta_0)$, (b) the gap-closing transition point $J = J_c$ $(= 1.77\Delta_0)$, and (c) the gapless TSC phase hosting MFEM $J > J_c$ $(= 2.0\Delta_0)$. (d) TDOS $\rho(E)$ is shown as a function of E/Δ_0 for the above-mentioned J values in the parentheses. All remaining parameters take values $g_x = g_y = \pi/2$, $\mu = \Delta_0 = t$.

[61]. We depict the bulk band structure of $\tilde{H}_{\rm L}(\mathbf{k})$ and the corresponding total density of states (TDOS) $\rho(E)$ in Fig. 2. The topological phase transition occurs between a normal SC phase with a trivial gap, Fig. 2(a) for $J < J_c$ to the gapless TSC phase, Fig. 2(c) for $J > J_c$ via a gap-closing phase, Fig. 2(b) at $J = J_c = 1.77\Delta_0$. The topological characterization via appropriate topological invariant (ν) is provided in the SM, Sec. S1 [61]. The invariant ν changes from 0 to 1 and hence, the system undergoes a transition from a trivial gapped state ($J < J_c$) to a nontrivial ($J > J_c$) TSC phase. This gapless phase displays graphenelike semimetalic behavior [62,63] where $\rho(E)$ corresponding to the gapless TSC phase ($J > J_c$) varies almost linearly with E, see Fig. 2(d). The band structure illustrated in Fig. 2(c) resembles that of the 2D-KM in the TSC phase, reported recently in Refs. [51,52]. There, the idea of 2D-KM hosting MFEM has been analytically formulated considering $(p_x + p_y)$ SCs. Indeed, we derive an effective "$p_x + p_y$" SC pairing [based on Eq. (3)] as a result of a domain of SS states propagating along the [110] direction when it is proximitized with an s-wave SC, see details in Sec. S6 in the SM [61]. Moreover, the inclusion of Rashba SOC in our model and the extension to multiorbitals [64,65] (see Sec. S7 in the SM [61]) do not significantly affect the presence and characteristics of MFEMs. These results seemingly ensure that the crucial prerequisite for the TSC phase is the noncollinear SS state stabilized in TM/SC systems.

In a slab geometry, we then calculate the spectral function $\mathcal{A}(k_x, \omega)$ [66]. Figure 3 shows the behavior of $\mathcal{A}(k_x, \omega)$ as a function of energy ω/Δ_0. Indeed, the MFEM signature is found clearly in the gapless TSC phase in Fig. 3(c). Figure 3(a) shows a trivial gap, i.e., without any signature of MFEM and in Fig. 3(b) for $J = J_c$, the edge modes in $\mathcal{A}(k_x, \omega)$ plot are still infinitesimally gaped. Experimentally, one can probe these signatures of TSC phase using ARPES

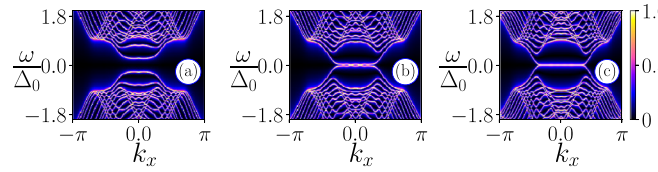

FIG. 3. Panels (a)–(c), the density plots of $\mathcal{A}(k_x, \omega)$ in the k_x-ω plane. A signature of the MFEM is seen in panel (c) for $J > J_c$ $(= 2.0\Delta_0)$ where the bulk is a gapless TSC. We choose the same set of respective parameters as mentioned in Fig. 2.

measurements but such a small gap close to the transition point will be impossible to resolve.

2D Kitaev lattice model for TM/SC heterostructure. Focusing on realistic materials framework, we rationalize the above-described phenomena using their magnetic ground states. We, therefore, design two prototype TM/SC heterostructures based on $3d$-TM monolayer grown on s-wave SC substrates: Mn/Nb(110) and Cr/Nb(001). The Mn/Nb(110) example with its relaxed-film geometry constructed with the optimized lattice constant of bulk Nb [67] indeed show a $c(2 \times 2)$ AFM order as the ground state (for detailed results, see SM, Sec. S3(A) [61]), recently reported in experiment also [56]. Surprisingly, we find a transition to an AFM-SS state via a uniform biaxial compressive strain within the range ~ -1 to -4%. Considering $a = 3.234$ Å and $b = \sqrt{a} = 4.574$ Å (strain $\sim -2.7\%$), Fig. 4(a) illustrates $\mathcal{J}_{ij}$'s and the absolute values of DMI ($\mathcal{D}_{ij}$) as a function of distance between Mn atoms and here, $\mathcal{K}$ is positive, i.e., out of plane. The vector orientations of DMIs in the inset connecting neighboring atoms match the symmetry rules for a system with $\mathcal{C}_{2v}$ symmetry [68]. Calculational details and more results with varying planner strains on Mn/Nb(110) film are provided in the SM, Sec. S3(B) [61]. The AFM-SS solution occurs as the stable state even without DMIs, resulting from the strong frustration in $\mathcal{J}_{ij}$'s connecting Mn moments ($\mathcal{M}_{\rm Mn} = 3.53\ \mu_{\rm B}$). The significantly weak DMI strengths (< 0.5 meV) are attributed to the weak SOC in light atoms and here, it determines a right-handed cycloidal AFM-SS as the ground state propagating along the [010] direction, see Fig. 4(b).

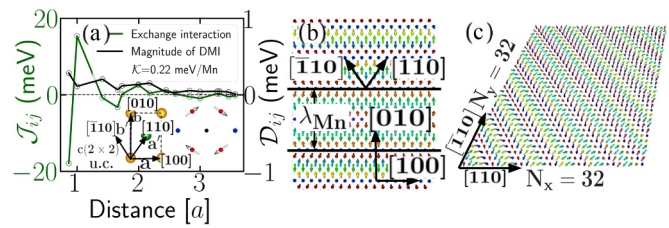

FIG. 4. For Mn/Nb(110) with strain $\sim -2.7\%$, (a) $\mathcal{J}_{ij}$'s and $\mathcal{D}_{ij}$'s are plotted as a function of distance measured in units of lattice constant a. Calculated $\mathcal{K}$ is out-of-plane. Lower left inset shows the $c(2 \times 2)$ AFM surface unit cell (yellow and green balls represent up and down spins, respectively), possessing $\mathcal{C}_{2v}$ symmetry. The lower right inset describes vector orientations of DMIs. (b) The AFM-SS ground state propagates along the [010] direction. (c) A 32×32 AFM-SS domain where edges are considered along [110] and [$\bar{1}$10] directions.

Here, we elucidate a minimal electronic-model Hamiltonian in real space for a 2D lattice:

$$H = -\sum_{\langle i,j\rangle,\alpha} t_{ij} c^{\dagger}_{i,\alpha} c_{j,\alpha} - \mu \sum_{i,\alpha} c^{\dagger}_{i,\alpha} c_{j,\alpha} + J \sum_{i,\alpha,\beta} c^{\dagger}_{i,\alpha} (\hat{\mathbf{s}}_i \cdot \boldsymbol{\sigma})_{\alpha,\beta} c_{i,\beta} + \Delta_0 \sum_i (c^{\dagger}_{i,\uparrow} c^{\dagger}_{i,\downarrow} + \text{H.c.}), \quad (4)$$

where i, j indices run over all the lattice sites, α, β denote the spin, $\langle\rangle$ represents nearest-neighbor hopping only, μ, J, Δ_0 represent the chemical potential, exchange coupling strength, s-wave SC gap, respectively, and $c^{\dagger}(c)$ corresponds to the electron creation (annihilation) operator for the SC. For simplicity, we assume the hopping amplitude $t_{ij} = t_{ji} = -t$ with $t = 1$ for the overall energy scale of our system. This minimal Hamiltonian is essentially constructed to ensure the importance of magnetic textures (alternative to the intrinsic SOC) of TM/SCs in the context of stabilizing TSC phase. All spin textures are actually entered in the third term in Eq. (4), describing a local interaction between the electron's spin (σ) and the moments of Mn or Cr. The unit vector $\hat{\mathbf{s}}_i$ denotes $(\sin\theta_i \cos\phi_i, \sin\theta_i \sin\phi_i, \cos\theta_i)$, mimicking locally varying magnetic impurities. One can extract these θ and ϕ from the spin textures generated by the MC simulations for TM/SC systems.

In the case of Mn/Nb(110), the $c(2 \times 2)$ AFM phase has been assessed first via numerically solving Eq. (4). Our results indeed describe the experimental findings where the s-wave SC and AFM phases are found to coexist [56], see the SM, Sec. S3(B) for more details [61]. The in-gap YSR bands ensure the qualitative accuracy of our minimal model in Eq. (4).

A few important results are obtained from the numerical simulations by considering the AFM-SS 2D domain. We construct a domain of size 32×32 (1024 spins) where the AFM-SS is propagating along the diagonal of that domain (as similar in the FM-SS, Fig. 1) with edges along [110] and [1$\bar{1}$0] directions, see Fig. 4(c). Hence, these directions are parallel to the rotated vectors $\mathbf{a}'$ and $\mathbf{b}'$ of the 2D lattice in the inset of Fig. 4(a). The measured θ and ϕ values describe $\hat{s}$ to solve Eq. (4), numerically. Results are summarized in Fig. 5, where (a) and (b) depict the local density of states (LDOS) for the zero-energy ($E = 0$) states using coupling constant $J = 4.5\Delta_0$ and $5.0\Delta_0$, respectively. The zero-energy states populate along the edges of the domain in Fig. 5(a) and hence, the system is in the TSC regime. The MFEM are maximally localized at the two opposite corners of the system and disperse gradually along the edges. Moreover, the signature of the MFEM is more evident from the nondispersive states at $E_n = 0$ in the eigenvalue spectrum plotted as a function of the state index n in the inset of Fig. 5(a). The semimetallic behavior of the bulk YSR band at $J = 4.5\Delta_0$ presented in the SM, Sec. S5 [61] for the TSC regime qualitatively matches with the continuum results presented in Fig. 2(d). The inset of Fig. 5(b) shows a trivial phase by opening a gap in the eigenvalue spectrum around $E_n = 0$.

Seemingly, it appears that the coupling constant J (rather, J/Δ_0) plays a major role in the phase transition between trivial SC and TSC phases. Particularly, J value is often very challenging to determine for such materials. Therefore, in Fig. 5(c), we depict the eigenvalue spectrum E/Δ_0 as a function of J/Δ_0 by employing open-boundary condition (OBC). The MFEM appears at zero energy between $J = 3.5\Delta_0$ and $J = 4.7\Delta_0$, indicating the TSC regime. We thereafter identify the parameter regime where the MFEM appears via calculating the bulk gap $\Delta G = |E_2\text{-}E_1|$, within periodic boundary condition (PBC). Here, E_1 (E_2) represents the two low-energy bands. We depict $\Delta G/\Delta_0$ in the J/Δ_0-μ/Δ_0 plane in Fig. 5(d). The gapless TSC regime harboring MFEM is highlighted by the dark blue strip ($\Delta G \simeq 0$), while the regime outside ($\Delta G > 0$) represents gapped trivial superconducting phase. In the inset of Fig. 5(d), we illustrate the bulk-gap ΔG as a function of J for a fixed value of μ, for the transparent visibility of the TSC regime. The bulk-gap ΔG vanishes in the topological regime and MFEM appears at the boundary.

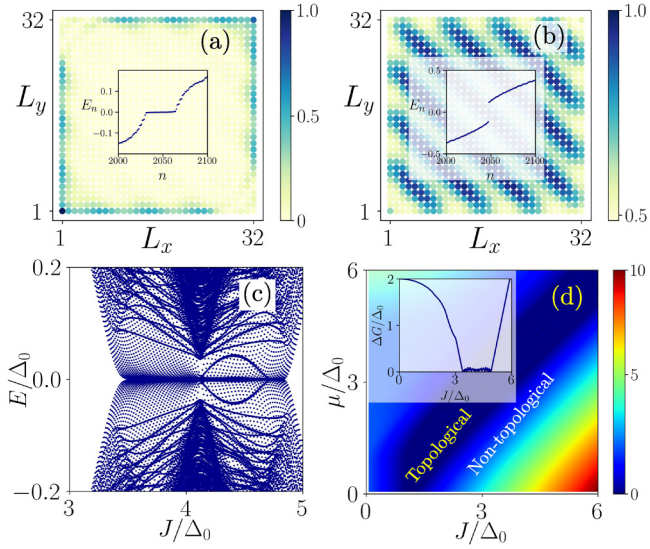

FIG. 5. The normalized LDOS for $E = 0$ eigenstate, computed within a spin-lattice model of size 32×32 spins (L_x-L_y square plane). Here, 2D lattice points are defined in units of $\mathbf{a}'$ and $\mathbf{b}'$, as shown in the inset of Fig. 4(a). For Mn/Nb(110) with AFM-SS state, (a) we identify the TSC phase for $J = 4.5\Delta_0$. The LDOS is predominantly localized at the domain edges denoting MFEMs. (b) In the trivial phase for $J = 5.0\Delta_0$, LDOS is delocalized over the entire domain. Insets in (a) and (b) show a zero-energy flat mode and a trivial gap in the eigenvalue E_n vs state n plots, respectively. (c) Energy eigenvalues E of H is shown as a function of J using OBC. (d) The bulk-gap ΔG profile is shown in the J-μ plane employing PBC, indicating the TSC phase (dark blue regime). The inset is showing ΔG vs J plot for a fixed μ ($= 4.0\Delta_0$ and $\Delta_0 = t$).

The new example, Cr/Nb(001), shows left-handed cycloidal AFM-SS as the ground state without strain, propagating along both [100] and [010] degenerate directions. The degeneracy is owing to the symmetry rules followed by the DMI vectors in the $\mathcal{C}_{4v}$ symmetric film [68]. We solve Eq. (4) again for the square domains and all results are presented in the SM, Sec. S4 [61].

Summary and outlook. In conclusion, by employing a continuum model, we demonstrate a route to generate a gapless TSC phase hosting MFEMs by engineering noncollinear SS state proximitized with an s-wave superconductor. This under-

lying scheme is later extended within a minimal lattice model which provides a unique way to unveil the TSC phase in prototype real TM/SC (*s*-wave) materials: Mn/Nb(110) under strain and Cr/Nb(001). Even though the SOC strength in Nb is expected to be very small, the AFM-SS can be stabilized from the exchange frustration, particularly in the Mn/Nb(110) sample and, thereby, an effective SOC and Zeeman field terms due to the spin textures manifest the Hamiltonian obtained in Eq. (3). The immobile MFEMs can be thought of as edge channels to carry edge vortices in Josephson junction geometries—offering a possibility for non-Abelian "braiding" operations [69,70]. Note that a similar idea has been demonstrated in the context of braiding mobile vortices via the chiral dispersive edge channels in 2D [71]. Importantly, the investigation of this "braiding" protocol for MFEMs is an intriguing and important direction for future studies. Indeed, our realistic model Hamiltonian unveils excellent examples where the strain-driven modulation of the noncollinear magnetic phases can offer unprecedented control over various types of TSC phases including 2D-KM, higher-order topological superconductors [72], and AFM-SC spintronics [73] in the near future.

Acknowledgments. The first-principle calculations in this letter are supported by the Swedish National Infrastructure for Computing (SNIC) facility and for that, S.B. and A.K.N. sincerely thank Professor P. M. Oppeneer. P.C., S.B., A.K.G., A.S., and A.K.N. acknowledge the support from Department of Atomic Energy (DAE), Govt. of India. S.B. and A.K.N. acknowledge the KALINGA HPC facility at NISER, Bhubaneswar, and P.C., A.K.G., and A.S. acknowledge the SAMKHYA: HPC Facility provided at IOP, Bhubaneswar, for numerical computations.

[1] A. Y. Kitaev, Unpaired Majorana fermions in quantum wires, Phys. Usp. **44**, 131 (2001).
[2] D. A. Ivanov, Non-Abelian statistics of half-quantum vortices in *p*-wave superconductors, Phys. Rev. Lett. **86**, 268 (2001).
[3] C. Nayak, S. H. Simon, A. Stern, M. Freedman, and S. Das Sarma, Non-Abelian anions and topological quantum computation, Rev. Mod. Phys. **80**, 1083 (2008).
[4] A. Kitaev, Periodic table for topological insulators and superconductors, AIP Conf. Proc. **1134**, 22 (2009).
[5] X.-L. Qi and S.-C. Zhang, Topological insulators and superconductors, Rev. Mod. Phys. **83**, 1057 (2011).
[6] J. Alicea, New directions in the pursuit of Majorana fermions in solid state systems, Rep. Prog. Phys. **75**, 076501 (2012).
[7] M. Leijnse and K. Flensberg, Introduction to topological superconductivity and Majorana fermions, Semicond. Sci. Technol. **27**, 124003 (2012).
[8] C. Beenakker, Search for Majorana fermions in superconductors, Annu. Rev. Condens. Matter Phys. **4**, 113 (2013).
[9] R. Aguado, Majorana quasiparticles in condensed matter, Riv. Nuovo Cim. **40**, 523 (2017).
[10] F. Pientka, L. I. Glazman, and F. von Oppen, Topological superconducting phase in helical Shiba chains, Phys. Rev. B **88**, 155420 (2013).
[11] S. Nadj-Perge, I. K. Drozdov, B. A. Bernevig, and A. Yazdani, Proposal for realizing Majorana fermions in chains of magnetic atoms on a superconductor, Phys. Rev. B **88**, 020407(R) (2013).
[12] J. Klinovaja, P. Stano, A. Yazdani, and D. Loss, Topological superconductivity and Majorana fermions in RKKY systems, Phys. Rev. Lett. **111**, 186805 (2013).
[13] B. Braunecker and P. Simon, Interplay between classical magnetic moments and superconductivity in quantum one-dimensional conductors: Toward a self-sustained topological Majorana phase, Phys. Rev. Lett. **111**, 147202 (2013).
[14] M. M. Vazifeh and M. Franz, Self-organized topological state with Majorana fermions, Phys. Rev. Lett. **111**, 206802 (2013).
[15] J. D. Sau and E. Demler, Bound states at impurities as a probe of topological superconductivity in nanowires, Phys. Rev. B **88**, 205402 (2013).
[16] F. Pientka, L. I. Glazman, and F. von Oppen, Unconventional topological phase transitions in helical Shiba chains, Phys. Rev. B **89**, 180505(R) (2014).
[17] K. Pöyhönen, A. Westström, J. Röntynen, and T. Ojanen, Majorana states in helical Shiba chains and ladders, Phys. Rev. B **89**, 115109 (2014).
[18] I. Reis, D. J. J. Marchand, and M. Franz, Self-organized topological state in a magnetic chain on the surface of a superconductor, Phys. Rev. B **90**, 085124 (2014).
[19] W. Hu, R. T. Scalettar, and R. R. P. Singh, Interplay of magnetic order, pairing, and phase separation in a one-dimensional spin-fermion model, Phys. Rev. B **92**, 115133 (2015).
[20] H.-Y. Hui, P. M. R. Brydon, J. D. Sau, S. Tewari, and S. D. Sarma, Majorana fermions in ferromagnetic chains on the surface of bulk spin-orbit coupled *s*-wave superconductors, Sci. Rep. **5**, 8880 (2015).
[21] S. Hoffman, J. Klinovaja, and D. Loss, Topological phases of inhomogeneous superconductivity, Phys. Rev. B **93**, 165418 (2016).
[22] M. H. Christensen, M. Schecter, K. Flensberg, B. M. Andersen, and J. Paaske, Spiral magnetic order and topological superconductivity in a chain of magnetic adatoms on a two-dimensional superconductor, Phys. Rev. B **94**, 144509 (2016).
[23] G. Sharma and S. Tewari, Yu-Shiba-Rusinov states and topological superconductivity in Ising paired superconductors, Phys. Rev. B **94**, 094515 (2016).
[24] G. M. Andolina and P. Simon, Topological properties of chains of magnetic impurities on a superconducting substrate: Interplay between the shiba band and ferromagnetic wire limits, Phys. Rev. B **96**, 235411 (2017).
[25] A. Theiler, K. Björnson, and A. M. Black-Schaffer, Majorana bound state localization and energy oscillations for magnetic impurity chains on conventional superconductors, Phys. Rev. B **100**, 214504 (2019).
[26] D. Sticlet and C. Morari, Topological superconductivity from magnetic impurities on monolayer $NbSe_2$, Phys. Rev. B **100**, 075420 (2019).

[27] M. Mashkoori and A. Black-Schaffer, Majorana bound states in magnetic impurity chains: Effects of d-wave pairing, Phys. Rev. B **99**, 024505 (2019).

[28] G. C. Mnard, C. Brun, R. Leriche, M. Trif, F. Debontridder, D. Demaille, D. Roditchev, P. Simon, and T. Cren, Yu-Shiba-Rusinov bound states versus topological edge states in Pb/Si(111), Eur. Phys. J.: Spec. Top. **227**, 2303 (2019).

[29] M. Mashkoori, S. Pradhan, K. Björnson, J. Fransson, and A. M. Black-Schaffer, Identification of topological superconductivity in magnetic impurity systems using bulk spin polarization, Phys. Rev. B **102**, 104501 (2020).

[30] R. L. R. C. Teixeira, D. Kuzmanovski, A. M. Black-Schaffer, and L. G. G. V. D. da Silva, Enhanced Majorana bound states in magnetic chains on superconducting topological insulator edges, Phys. Rev. B **102**, 165312 (2020).

[31] S. Rex, I. V. Gornyi, and A. D. Mirlin, Majorana modes in emergent-wire phases of helical and cycloidal magnet-superconductor hybrids, Phys. Rev. B **102**, 224501 (2020).

[32] V. Perrin, M. Civelli, and P. Simon, Identifying Majorana bound states by tunneling shot-noise tomography, Phys. Rev. B **104**, L121406 (2021).

[33] H. Shiba, Classical spins in superconductors, Prog. Theor. Phys. **40**, 435 (1968).

[34] V. Kaladzhyan, C. Bena, and P. Simon, Asymptotic behavior of impurity-induced bound states in low-dimensional topological superconductors, J. Phys.: Condens. Matter **28**, 485701 (2016).

[35] N. Dai, K. Li, Y.-B. Yang, and Y. Xu, Topological quantum phase transitions in metallic Shiba lattices, Phys. Rev. B **106**, 115409 (2022).

[36] J. Ortuzar, S. Trivini, M. Alvarado, M. Rouco, J. Zaldivar, A. L. Yeyati, J. I. Pascual, and F. S. Bergeret, Yu-Shiba-Rusinov states in two-dimensional superconductors with arbitrary Fermi contours, Phys. Rev. B **105**, 245403 (2022).

[37] A. Ghazaryan, A. Kirmani, R. M. Fernandes, and P. Ghaemi, Anomalous Shiba states in topological iron-based superconductors, Phys. Rev. B **106**, L201107 (2022).

[38] H. Schmid, J. F. Steiner, K. J. Franke, and F. von Oppen, Quantum Yu-Shiba-Rusinov dimers, Phys. Rev. B **105**, 235406 (2022).

[39] P. Chatterjee, S. Pradhan, A. K. Nandy, and A. Saha, Tailoring the phase transition from topological superconductor to trivial superconductor induced by magnetic textures of a spin chain on a p-wave superconductor, Phys. Rev. B **107**, 085423 (2023).

[40] A. Yazdani, B. A. Jones, C. P. Lutz, M. F. Crommie, and D. M. Eigler, Probing the local effects of magnetic impurities on superconductivity, Science **275**, 1767 (1997).

[41] A. Yazdani, C. M. Howald, C. P. Lutz, A. Kapitulnik, and D. M. Eigler, Impurity-induced bound excitations on the surface of $Bi_2Sr_2CaCu_2O_8$, Phys. Rev. Lett. **83**, 176 (1999).

[42] A. Yazdani, Visualizing Majorana fermions in a chain of magnetic atoms on a superconductor, Phys. Scr. **T164**, 014012 (2015).

[43] L. Schneider, P. Beck, T. Posske, D. Crawford, E. Mascot, S. Rachel, R. Wiesendanger, and J. Wiebe, Topological Shiba bands in artificial spin chains on superconductors, Nat. Phys. **17**, 943 (2021).

[44] P. Beck, L. Schneider, L. Rózsa, K. Palotás, A. Lászlóffy, L. Szunyogh, J. Wiebe, and R. Wiesendanger, Spin-orbit coupling induced splitting of Yu-Shiba-Rusinov states in antiferromagnetic dimers, Nat. Commun. **12**, 2040 (2021).

[45] D. Wang, J. Wiebe, R. Zhong, G. Gu, and R. Wiesendanger, Spin-polarized Yu-Shiba-Rusinov states in an iron-based superconductor, Phys. Rev. Lett. **126**, 076802 (2021).

[46] L. Schneider, P. Beck, J. Neuhaus-Steinmetz, L. Rózsa, T. Posske, J. Wiebe, and R. Wiesendanger, Precursors of Majorana modes and their length-dependent energy oscillations probed at both ends of atomic shiba chains, Nat. Nanotechnol. **17**, 384 (2022).

[47] J. Li, H. Chen, I. K. Drozdov, A. Yazdani, B. A. Bernevig, and A. H. MacDonald, Topological superconductivity induced by ferromagnetic metal chains, Phys. Rev. B **90**, 235433 (2014).

[48] P. M. R. Brydon, S. Das Sarma, H.-Y. Hui, and J. D. Sau, Topological Yu-Shiba-Rusinov chain from spin-orbit coupling, Phys. Rev. B **91**, 064505 (2015).

[49] J. Rontynen and T. Ojanen, Topological superconductivity and high Chern numbers in 2D ferromagnetic Shiba lattices, Phys. Rev. Lett. **114**, 236803 (2015).

[50] J. Röntynen and T. Ojanen, Chern mosaic: Topology of chiral superconductivity on ferromagnetic adatom lattices, Phys. Rev. B **93**, 094521 (2016).

[51] P. Wang, S. Lin, G. Zhang, and Z. Song, Topological gapless phase in Kitaev model on square lattice, Sci. Rep. **7**, 17179 (2017).

[52] K. L. Zhang, P. Wang, and Z. Song, Majorana flat band edge modes of topological gapless phase in 2D Kitaev square lattice, Sci. Rep. **9**, 4978 (2019).

[53] N. Sedlmayr, J. M. Aguiar-Hualde, and C. Bena, Flat Majorana bands in two-dimensional lattices with inhomogeneous magnetic fields: Topology and stability, Phys. Rev. B **91**, 115415 (2015).

[54] S. Nakosai, Y. Tanaka, and N. Nagaosa, Two-dimensional p-wave superconducting states with magnetic moments on a conventional s-wave superconductor, Phys. Rev. B **88**, 180503(R) (2013).

[55] W. Chen and A. P. Schnyder, Majorana edge states in superconductor-noncollinear magnet interfaces, Phys. Rev. B **92**, 214502 (2015).

[56] R. Lo Conte, M. Bazarnik, K. Palotás, L. Rózsa, L. Szunyogh, A. Kubetzka, K. von Bergmann, and R. Wiesendanger, Coexistence of antiferromagnetism and superconductivity in Mn/Nb(110), Phys. Rev. B **105**, L100406 (2022).

[57] A. K. Nandy, N. S. Kiselev, and S. Blügel, Interlayer exchange coupling: A general scheme turning chiral magnets into magnetic multilayers carrying atomic-scale skyrmions, Phys. Rev. Lett. **116**, 177202 (2016).

[58] R. Lo Conte, A. K. Nandy, G. Chen, A. L. Fernandes Cauduro, A. Maity, C. Ophus, Z. Chen, A. T. N'Diaye, K. Liu, A. K. Schmid, and R. Wiesendanger, Tuning the properties of zero-field room temperature ferromagnetic skyrmions by interlayer exchange coupling, Nano Lett. **20**, 4739 (2020).

[59] M. Bode, M. Heide, K. von Bergmann, P. Ferriani, S. Heinze, G. Bihlmayer, A. Kubetzka, O. Pietzsch, S. Blügel, and R. Wiesendanger, Chiral magnetic order at surfaces driven by inversion asymmetry, Nature (London) **447**, 190 (2007).

[60] R. Hess, H. F. Legg, D. Loss, and J. Klinovaja, Prevalence of trivial zero-energy subgap states in nonuniform helical spin chains on the surface of superconductors, Phys. Rev. B **106**, 104503 (2022).

[61] See Supplemental Material at http://link.aps.org/supplemental/10.1103/PhysRevB.109.L121301 for the details of the topological characterization, methodology incuding *ab initio* electronic structure calculations using VASP and KKR-GF and atomistic spin–dynamics simulations, results in detail of the strain effect in Mn/Nb(110) example, full details of the new candidate Cr/Nb(001), semimetallic behavior details, derivation of an effective "$p_x + p_y$"-wave pairing and the effect of Rashba SOC in single and multiorbital scenarios, which includes Refs. [3,49,53,56,58,59,64,65,68–71,74–99].

[62] A. H. Castro Neto, F. Guinea, N. M. R. Peres, K. S. Novoselov, and A. K. Geim, The electronic properties of graphene, Rev. Mod. Phys. **81**, 109 (2009).

[63] K. Wakabayashi, K. ichi Sasaki, T. Nakanishi, and T. Enoki, Electronic states of graphene nanoribbons and analytical solutions, Sci Technol Adv. Mater. **11**, 054504 (2010).

[64] C. Liu, T. L. Hughes, X.-L. Qi, K. Wang, and S.-C. Zhang, Quantum spin Hall effect in inverted type-II semiconductors, Phys. Rev. Lett. **100**, 236601 (2008).

[65] L. Ortiz, R. A. Molina, G. Platero, and A. M. Lunde, Generic helical edge states due to Rashba spin-orbit coupling in a topological insulator, Phys. Rev. B **93**, 205431 (2016).

[66] The spectral function $\mathcal{A}(k_x, \omega)$ has been defined through the zero-temperature Green's function $\hat{G}(k_x, \omega)$ as $\mathcal{A}(k_x, \omega) = -\frac{1}{\pi}\mathrm{Im}[\mathrm{Tr}\{\hat{G}(k_x, \omega)\}]$, where $\hat{G}(k_x, \omega) = [\mathbb{I} - \tilde{H}_{\mathrm{L}}(y, k_x)]^{-1}$.

[67] Within the generalized gradient approximation (GGA) functional, the optimized lattice constant of bulk body-centered-cubic Nb is found to be $a_{\mathrm{Nb}} = 3.3232$ Å, an excellent agreement with the experimental value of about 3.32 Å [74]. The value of a_{Nb} is then used to construct the optimized film geometry and also strains are measured with respect to a_{Nb}.

[68] T. Moriya, Anisotropic superexchange interaction and weak ferromagnetism, Phys. Rev. **120**, 91 (1960).

[69] J. Alicea, Y. Oreg, G. Refael, F. von Oppen, and M. P. A. Fisher, Non-Abelian statistics and topological quantum information processing in 1D wire networks, Nat. Phys. **7**, 412 (2011).

[70] G. L. Fatin, A. Matos-Abiague, B. Scharf, and I. Žutić, Wireless Majorana bound states: From magnetic tunability to braiding, Phys. Rev. Lett. **117**, 077002 (2016).

[71] C. W. J. Beenakker, P. Baireuther, Y. Herasymenko, I. Adagideli, L. Wang, and A. R. Akhmerov, Deterministic creation and braiding of chiral edge vortices, Phys. Rev. Lett. **122**, 146803 (2019).

[72] A. K. Ghosh, T. Nag, and A. Saha, Hierarchy of higher-order topological superconductors in three dimensions, Phys. Rev. B **104**, 134508 (2021).

[73] L. Salemi, M. Berritta, A. K. Nandy, and P. M. Oppeneer, Orbitally dominated Rashba-Edelstein effect in noncentrosymmetric antiferromagnets, Nat. Commun. **10**, 5381 (2019).

[74] A. Jain, S. P. Ong, G. Hautier, W. Chen, W. D. Richards, S. Dacek, S. Cholia, D. Gunter, D. Skinner, G. Ceder, and K. A. Persson, Commentary: The Materials Project: A materials genome approach to accelerating materials innovation, APL Mater. **1**, 011002 (2013).

[75] I. Dzyaloshinsky, A thermodynamic theory of "weak" ferromagnetism of antiferromagnetics, J. Phys. Chem. Solids **4**, 241 (1958).

[76] G. P. Müller, M. Hoffmann, C. Dißelkamp, D. Schürhoff, S. Mavros, M. Sallermann, N. S. Kiselev, H. Jónsson, and S. Blügel, Spirit: Multifunctional framework for atomistic spin simulations, Phys. Rev. B **99**, 224414 (2019).

[77] P. D. Landau and K. Binder, *A Guide to Monte Carlo Methods in Statistical Physics* (Cambridge University Press, Cambridge, England, 2000).

[78] P. J. Van Laarhoven and E. H. Aarts, *Simulated Annealing: Theory and Applications* (D. Reidel, Dordrecht, Holland, 1987).

[79] C. Heo, N. S. Kiselev, A. K. Nandy, S. Blügel, and T. Rasing, Switching of chiral magnetic skyrmions by picosecond magnetic field pulses via transient topological states, Sci. Rep. **6**, 27146 (2016).

[80] V. Flovik, A. Qaiumzadeh, A. K. Nandy, C. Heo, and T. Rasing, Generation of single skyrmions by picosecond magnetic field pulses, Phys. Rev. B **96**, 140411(R) (2017).

[81] B. Lian, X.-Q. Sun, A. Vaezi, X.-L. Qi, and S.-C. Zhang, Topological quantum computation based on chiral Majorana fermions, Proc. Natl. Acad. Sci. **115**, 10938 (2018).

[82] S. Bera and S. S. Mandal, Skyrmions at vanishingly small Dzyaloshinskii-Moriya interaction or zero magnetic field, J. Phys.: Condens. Matter **33**, 255801 (2021).

[83] S. Bera and S. S. Mandal, Theory of the skyrmion, meron, antiskyrmion, and antimeron in chiral magnets, Phys. Rev. Res. **1**, 033109 (2019).

[84] M. Sato, Y. Takahashi, and S. Fujimoto, Non-Abelian topological order in s-wave superfluids of ultracold fermionic atoms, Phys. Rev. Lett. **103**, 020401 (2009).

[85] M. Sato, Y. Takahashi, and S. Fujimoto, Non-Abelian topological orders and Majorana fermions in spin-singlet superconductors, Phys. Rev. B **82**, 134521 (2010).

[86] J. Hafner, *Ab initio* simulations of materials using VASP: Density-functional theory and beyond, J. Comput. Chem. **29**, 2044 (2008).

[87] G. Kresse and J. Furthmüller, Efficiency of *ab initio* total energy calculations for metals and semiconductors using a plane-wave basis set, Comput. Mater. Sci. **6**, 15 (1996).

[88] G. Kresse and J. Furthmüller, Efficient iterative schemes for *ab initio* total-energy calculations using a plane-wave basis set, Phys. Rev. B **54**, 11169 (1996).

[89] J. P. Perdew, K. Burke, and M. Ernzerhof, Generalized gradient approximation made simple, Phys. Rev. Lett. **77**, 3865 (1996).

[90] G. Kresse and D. Joubert, From ultrasoft pseudopotentials to the projector augmented-wave method, Phys. Rev. B **59**, 1758 (1999).

[91] P. E. Blöchl, Projector augmented-wave method, Phys. Rev. B **50**, 17953 (1994).

[92] D. S. G. Bauer, Development of a relativistic full-potential first-principles multiple scattering Green function method applied to complex magnetic textures of nano structures at surfaces. Ph.D. Thesis, RWTH Aachen, 2013.

[93] A. I. Liechtenstein, M. I. Katsnelson, V. P. Antropov, and V. A. Gubanov, Local spin density functional approach to the theory of exchange interactions in ferromagnetic metals and alloys, J. Magn. Magn. Mater. **67**, 65 (1987).

[94] J. Zabloudil, R. Hammerling, L. Szunyogh, and P. Weinberger, *Electron Scattering in Solid Matter: A Theoretical and Computational Treatise* (Springer Berlin, Heidelberg, 2005).

[95] S. H. Vosko, L. Wilk, and M. Nusair, Accurate spin-dependent electron liquid correlation energies for local spin density calculations: a critical analysis, Can. J. Phys. **58**, 1200 (1980).

[96] L. Udvardi, L. Szunyogh, K. Palotás, and P. Weinberger, First-principles relativistic study of spin waves in thin magnetic films, Phys. Rev. B **68**, 104436 (2003).

[97] H. Ebert and S. Mankovsky, Anisotropic exchange coupling in diluted magnetic semiconductors: *Ab initio* spin-density functional theory, Phys. Rev. B **79**, 045209 (2009).

[98] A. Fert and P. M. Levy, Role of anisotropic exchange interactions in determining the properties of spin-glasses, Phys. Rev. Lett. **44**, 1538 (1980).

[99] P. Ferriani, K. von Bergmann, E. Y. Vedmedenko, S. Heinze, M. Bode, M. Heide, G. Bihlmayer, S. Blügel, and R. Wiesendanger, Atomic-scale spin spiral with a unique rotational sense: Mn monolayer on W(001), Phys. Rev. Lett. **101**, 027201 (2008).